Different Precipitation Systems between Hiroshima and Keihanshin during Extreme Rainfall Event in Western Japan in July 2018

Sueki, Kenta

Kajikawa, Yoshiyuki

(Citation)
Journal of the Meteorological Society of Japan. Ser. II,97(6):1221-1232

(Issue Date)
2019-12

(Resource Type)
journal article

(Version)
Version of Record

(URL)
https://hdl.handle.net/20.500.14094/90007287

Journal of the Meteorological Society of Japan, **97**(6), 1221−1232, 2019. doi:10.2151/jmsj.2019-063
Special Edition on Extreme Rainfall Events in 2017 and 2018

NOTES AND CORRESPONDENCE

Different Precipitation Systems between Hiroshima and Keihanshin during Extreme Rainfall Event in Western Japan in July 2018

Kenta SUEKI

RIKEN Center for Computational Science, Kobe, Japan
RIKEN Cluster for Pioneering Research, Kobe, Japan

and

Yoshiyuki KAJIKAWA

RIKEN Center for Computational Science, Kobe, Japan
Research Center for Urban Safety and Security, Kobe University, Kobe, Japan

(Manuscript received 16 March 2019, in final form 26 August 2019)

Abstract

During the recent catastrophic heavy rainfall event in western Japan in July 2018, both the Hiroshima and Keihanshin areas were subjected to unusual total rainfall amounts in 72 hours from 1200 UTC 4 July to 1200 UTC 7 July. However, the number of sediment disasters was significantly larger in the Hiroshima area. We explore possible reasons for this difference in the sediment disaster occurrences between the Hiroshima and Keihanshin areas, focusing on the different rainfall characteristics in these two areas during the heavy rainfall event. Based on the radar observations, we investigate the characteristics of precipitation systems striking the Hiroshima and Keihanshin areas and find that significantly large precipitation systems, with areas equal to or larger than 10^4 km^2, dominated the Hiroshima area, causing rapid accumulation of the rainfall amount and enhancing the risk of deadly sediment disasters in this area. On the other hand, in the Keihanshin area, moderately intense rainfall and relatively small precipitation systems were dominant. We suggest that the difference in the amount of damage between the Hiroshima and Keihanshin areas was mainly caused by the differently-sized precipitation systems striking these two areas. Statistics relating to the background atmospheric conditions for the precipitation systems in the heavy rainfall event reveal that a high vertical wind shear environment provides preferable conditions for the formation of large precipitation systems.

Keywords heavy rainfall; precipitation system; vertical wind shear; radar observation

Citation Sueki, K., and Y. Kajikawa, 2019: Different Precipitation Systems between Hiroshima and Keihanshin during Extreme Rainfall Event in Western Japan in July 2018. *J. Meteor. Soc. Japan*, **97**, 1221–1232, doi:10.2151/jmsj.2019-063.

Corresponding author: Kenta Sueki, RIKEN Center for Computational Science, 7-1-26 Minatojima-minami-machi, Chuo-ku, Kobe, Hyogo 650-0047, Japan
E-mail: kenta.sueki@riken.jp
J-stage Advance Published Date: 6 September 2019

1. Introduction

In the beginning of July 2018, many areas of Japan were subjected to extremely heavy rainfall. More than 200 people were killed during this event, which has been recorded as one of the worst casualties caused by a single rainfall event in the past 30 years in Japan. The heavy rainfall areas and human casualties were particularly concentrated in western Japan. Figure 1a shows the time series of the total rainfall rate in western Japan during this event. Heavy rainfall occurred over 72 h from 1200 UTC 4 July to 1200 UTC 7 July. Figure 1b is a map of the accumulated rainfall over western Japan during these 72 hours. Northern Kyushu Island, Hiroshima area, central Shikoku Island, Keihanshin area, and Gifu area (labeled as 1–5 in Fig. 1b, respectively) were subjected to particularly large amounts of rainfall during the event. However, the climatological mean rainfall amounts in Kyushu and Shikoku Islands and the Gifu area are generally large in July—more than 400 mm—(Fig. 1c), thereby indicating that the rainfall amounts in July 2018 in these areas were not exceptional. On the other hand, the Hiroshima and Keihanshin areas experienced unusual rainfall in July 2018, considering the fact these areas normally experience relatively small climatological rainfall amounts. Thus, the Hiroshima and Keihanshin areas were prone to high risk of disaster caused by a rare heavy rainfall event.

However, the number of sediment disasters caused by the heavy rainfall was significantly different between the Hiroshima and Keihanshin areas. In Hiroshima Prefecture, there were 1,242 sediment disasters (609 debris flows, 1 landslide, and 632 slope failures), according to information provided by the Cabinet Office (2019). This caused catastrophic damage in Hiroshima Prefecture: 1,150 completely destroyed houses and 115 casualties with 5 missing people (Cabinet Office 2019). On the other hand, there were 113 sediment disasters (28 debris flows, 5 landslides, and 80 slope failures) in three prefectures in the Keihanshin area (Hyogo, Osaka, and Kyoto Prefectures) (Cabinet Office 2019). As a result, damage in these prefectures—34 completely destroyed houses and 7 casualties (Cabinet Office 2019)—was significantly smaller than it was in Hiroshima Prefecture. What was the cause of such a large difference in damage between the Hiroshima and Keihanshin areas although the rainfall amounts were almost the same? Explanations include differences in topography, geological features, and land use properties. However, the differences in the rainfall characteristics between the two areas should also be considered a potential primary factor leading to differences in damage. From the viewpoints of both scientific progress and disaster risk reduction, it is worth investigating what kind of rainfall is particularly hazardous and can cause catastrophic damage to human society.

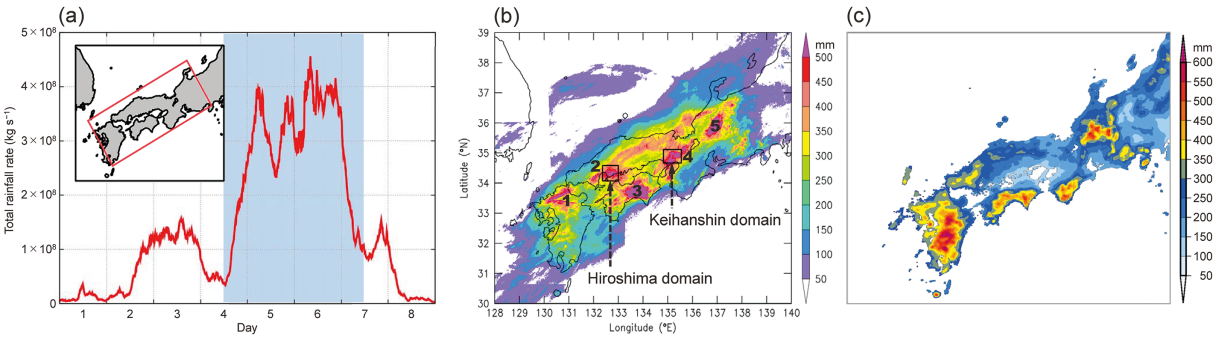

Fig. 1. (a) Time series of total rainfall rate in the red-framed region, shown in the map at the upper left, as estimated from the radar reflectivity observed by C-band radars operated by the Japan Meteorological Agency (JMA). The time range is from 0000 UTC 1 July 2018 (right) to 0000 UTC 9 July 2018 (left). The analysis period from 1200 UTC 4 July to 1200 UTC 7 July is indicated by the shaded box. (b) Accumulated rainfall amounts in the 72-h analysis period, as estimated from radar observations. The numbers in the map indicate five areas with large rainfall amounts during the 72 hours from 1200 UTC 4 July (1: northern Kyushu Island, 2: Hiroshima area, 3: central Shikoku Island, 4: Keihanshin area, and 5: Gifu area). The two boxes indicate the Hiroshima and Keihanshin domains analyzed in this study. (c) Thirty-year (1981–2010) climatological precipitation data made by the authors based on the monthly mean precipitation in July created by JMA (https://www.data.jma.go.jp/obd/stats/data/mdrr/atlas/precipitation_07.pdf).

Against this backdrop, in this study, we attempted to clarify the different rainfall characteristics between the Hiroshima and Keihanshin areas and to discuss the background atmospheric conditions affecting the differences. Since large precipitation systems, such as "line-shaped" precipitation systems, are known to cause heavy rainfall events in Japan (Tsuguti and Kato 2014), here, we focus on the size of the precipitation system and its relation to the outbreak of sediment disasters in the Hiroshima area. In our analysis, we select two rectangular domains located in the Hiroshima and Keihanshin areas shown in Fig. 1b. Both these domains have almost the same area and experienced the same 72-h total rainfall amount although the corresponding damages were significantly different. This paper is organized as follows: Section 2 describes the data used for our analysis and our methods for investigating the precipitation systems and their background atmospheric conditions. The results are presented in Section 3 and discussed in Section 4. Section 5 presents our conclusions and remarks.

2. Data and methods

2.1 Data

We used the rainfall intensity data, estimated from the radar reflectivity observed by C-band radars operated by the Japan Meteorological Agency, to detect precipitation systems and estimate rainfall amounts. The radar data resolution is 0.75′, 0.5′, and 10 min for longitude, latitude, and time directions, respectively. Here, we note that the rainfall intensity estimated by using only the radar reflectivity may differ slightly from the actual rainfall intensity. In the study, we compared rainfall amounts estimated from the radar data to amounts estimated from more accurate radar/rain-gauge-analyzed precipitation data (Nagata 2011) for the heavy rainfall in July 2018 (Fig. S1). The time series of the total rainfall rate in western Japan from 0000 UTC 1 July to 0000 UTC 9 July 2018 are almost indistinguishable between the two datasets (Fig. S1a). The total rainfall amounts in western Japan over 72 h from 1200 UTC 4 July are highly correlated in space between the two datasets (Figs. S1b, c). Since rainfall data with no temporal smoothing is preferable for detecting precipitation systems for each time instant, we used radar data in this study.

To estimate the background atmospheric fields during the heavy rainfall event, we used the mesoscale analysis (MA) data (Japan Meteorological Agency 2013). The MA data resolution is 0.125°, 0.1°, and 3 h for longitude, latitude, and time directions, respectively, and 16 pressure levels from 1000 to 100 hPa are provided. The MA reflects many observations such as surface observations, radiosonde observations, and satellite observations by using the data assimilation system based on the four-dimensional variational method (Japan Meteorological Agency 2013). Thus, we assume that the MA provides the most likely atmospheric fields for each location and time.

2.2 Detection of precipitation systems

In this study, a continuous rainfall area, wherein the rainfall intensity P is equal to or greater than 10 mm h^{-1}, is defined as one "precipitation system", following Unuma and Takemi (2016). Here, if two grids of $P \geq 10$ mm h^{-1} share a common edge, they are considered to lie in the same precipitation system. Using this definition, we detected precipitation systems of various sizes for every 10 min. The minimum size of the precipitation system corresponds to one grid area (about 1 km^2), while the detected maximum one has an area larger than 10^4 km^2. To quantify the contributions of differently-sized precipitation systems to total rainfall amounts, we classified the detected precipitation systems into four categories based on their horizontal areas S: $S < 10^2$ km^2, $S = 10^2$–10^3 km^2, $S = 10^3$–10^4 km^2, and $S \geq 10^4$ km^2. Figure 2 shows an example of precipitation system classification at 1200 UTC 6 July 2018. Precipitation systems of various sizes (indicated in blue, cyan, magenta, and yellow from small to large-size categories) are embedded in the moderate ($P < 10$ mm h^{-1}) rainfall areas (gray). At this time, a chain of relatively large precipitation systems, with areas equal to or larger than 10^3 km^2 (magenta and yellow objects in Fig. 2), ran from the southwest to the northeast through the Hiroshima area. On the other hand, in the Keihanshin area, moderate rainfall was dominant.

2.3 Indices of background atmospheric conditions

Background thermodynamic and wind profiles greatly affect the structure and evolution of convective storms (Weisman and Klemp 1982). Here, in order to study the differences in such background conditions among differently-sized precipitation systems, we examine certain indices calculated from the atmospheric profiles. As indices of instability for moist convection, we use convective available potential energy (CAPE) and the K-index (KI). CAPE is defined as

$$\mathrm{CAPE} = \int_{\mathrm{LFC}}^{\mathrm{EL}} g \frac{T_{\mathrm{v}}' - \bar{T}_{\mathrm{v}}}{\bar{T}_{\mathrm{v}}} \mathrm{d}z, \tag{1}$$

where T_{v}' denotes the virtual temperature of the lifted

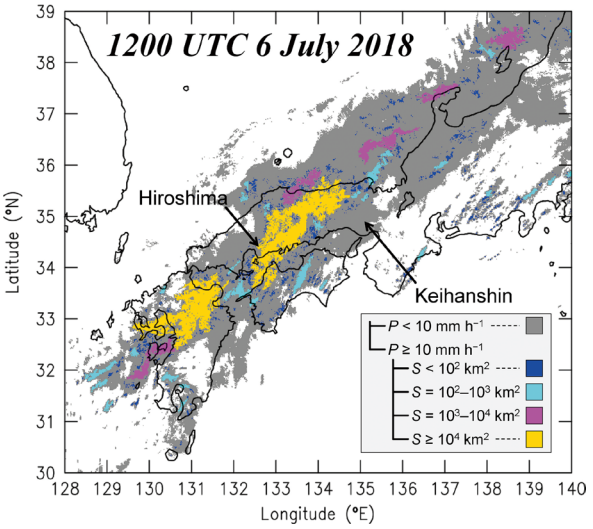

Fig. 2. Example of precipitation system classification at 1200 UTC 6 July 2018. Blue, cyan, magenta, and yellow colors correspond to precipitation systems of $S < 10^2$ km^2, $S = 10^2$–10^3 km^2, $S = 10^3$–10^4 km^2, and $S \geq 10^4$ km^2, respectively, where S denotes the area of the precipitation system. The gray color indicates moderate rain (rainfall intensity $P < 10$ mm h^{-1}).

parcel, $\overline{T}_v$ that of the background profile, and g the acceleration due to gravity. LFC and EL denote the level of free convection and the equilibrium level, respectively. We assume that the initial potential temperature and mixing ratio of the parcel are given as their averages over the lowest 500-m layer above ground level (AGL), respectively, because high equivalent potential temperature air in this layer is important for initiating severe moist convection (Kato 2018). KI is defined as

$$\mathrm{KI} = (T_{850} - T_{500}) + T_{\mathrm{d}850} - (T_{700} - T_{\mathrm{d}700}), \quad (2)$$

where T_{850}, T_{700}, and T_{500} denote the temperatures at 850, 700, and 500 hPa, respectively, and $T_{\mathrm{d}850}$ and $T_{\mathrm{d}700}$ indicate the dew point temperatures at 850 and 700 hPa, respectively. The first parenthetical term and $T_{\mathrm{d}850}$ indicate the temperature lapse rate and the low-level moisture, respectively, both of which contribute to conditional instability. The second parenthetical term indicates the mid-level dryness, which helps inhibit moist convection. Here, we note that this effect is not considered in the CAPE calculation. Regarding the vertical wind shear, we consider the wind difference between two particular levels:

$$\Delta V_{z_1-z_2} = \left[(u_{z_2} - u_{z_1})^2 + (v_{z_2} - v_{z_1})^2\right]^{1/2}, \quad (3)$$

where u_{z_1} and u_{z_2} indicate the zonal winds at z_1 and z_2 km AGL, respectively, and v_{z_1} and v_{z_2} the corresponding meridional winds at the same levels. In the present study, both low-level (0.5–2.5 km) and mid-level (2.5–6.0 km) vertical wind shears ($\Delta V_{0.5-2.5}$ and $\Delta V_{2.5-6.0}$) were examined. Some idealized numerical experiments showed that the lowest 2.5-km vertical wind shear, coupled with conditional instability, can generate long-lived squall lines (Rotunno et al. 1988; Weisman et al. 1988; Takemi 2006). Further, large vertical wind shear below 6-km AGL provides preferable conditions for intense, long-lasting convective storms with rotating updraft (Rasmussen and Blanchard 1998; Thompson et al. 2003) because the horizontal vorticity associated with vertical wind shear is tilted by convective updrafts to generate vertical vorticity (Wilhelmson and Klemp 1978; Rotunno 1981). Therefore, these layers' vertical wind shear can enhance the organization, longevity, and intensity of convective storms, thus leading to severe rainfall during the event. All indices were calculated by using the MA data.

2.4 Analysis domain

In the study, we compared the rainfall characteristics in the two rectangular domains located in the Hiroshima and Keihanshin areas (Fig. 1b). The Hiroshima domain is located between 132°21′45″–133°00′00″E and 34°04′30″–34°35′00″N, corresponding to an area of 3309 km^2. The Keihanshin domain is located between 134°49′30″–135°33′00″E and 34°40′00″–35°07′00″N, and its corresponding area is also 3309 km^2. The area-averaged total rainfall amount in the 72 hours from 1200 UTC 4 July 2018 estimated from radar data was 449 mm (460 mm) for the Hiroshima (Keihanshin) domain. Here, we note that the total rainfall amount estimated from the radar/rain-gauge-analyzed precipitation data was 422 mm both for the Hiroshima and Keihanshin domains (Fig. S2).

3. Results

3.1 Different precipitation systems between Hiroshima and Keihanshin areas

Figure 3 shows the time series of the area-averaged accumulated rainfall in the 72 hours from 1200 UTC 4 July to 1200 UTC 7 July 2018 for the Hiroshima and Keihanshin domains. To construct the figure, we decomposed the rainfall in the analysis domain into the five classes defined in Subsection 2.2: moderate

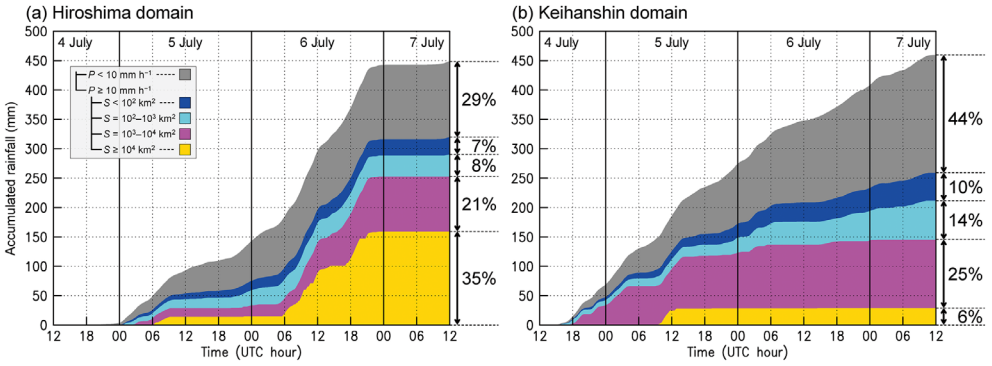

Fig. 3. Time series of area-averaged accumulated rainfall in the period from 1200 UTC 4 July to 1200 UTC 7 July 2018 both for (a) the Hiroshima domain, and (b) the Keihanshin domain, indicated by the black frames in Fig. 1b. The gray color indicates the contribution from moderate rain (rainfall intensity $P < 10$ mm h^{-1}). Blue, cyan, magenta, and yellow colors indicate contributions from precipitation systems with $S < 10^2$ km^2, $S = 10^2$–10^3 km^2, $S = 10^3$–10^4 km^2, and $S \geq 10^4$ km^2, respectively, where S denotes the area of the precipitation system. The percentages to the right of each graph indicate cumulative contribution rates for each classification.

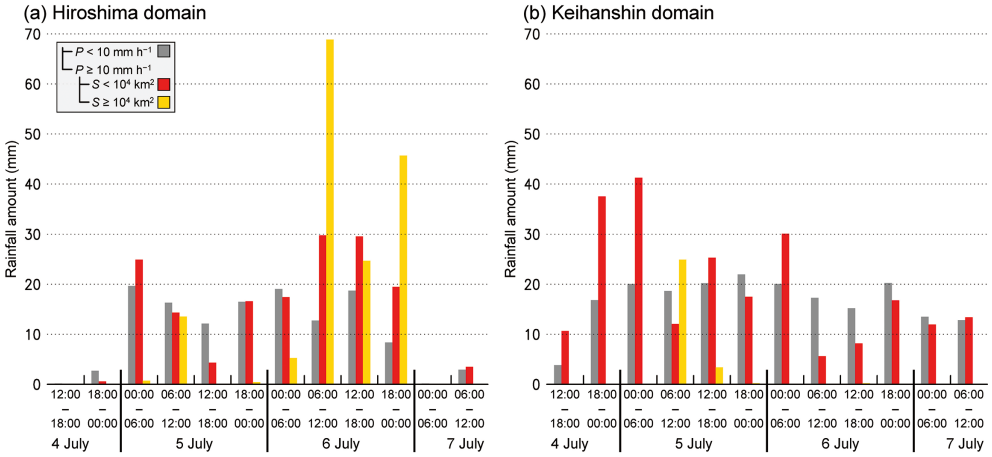

Fig. 4. Area-averaged rainfall amount for every 6 hours from 1200 UTC 4 July to 1200 UTC 7 July 2018 both for (a) the Hiroshima domain and (b) the Keihanshin domain. The gray bars show the rainfall amounts caused by moderate rain (rainfall intensity $P < 10$ mm h^{-1}). Red and yellow bars show rainfall amounts caused by precipitation systems with $S < 10^4$ km^2 and $S \geq 10^4$ km^2, respectively, where S denotes the area of the precipitation system.

rain ($P < 10$ mm h^{-1}) and severe rain ($P \geq 10$ mm h^{-1}) associated with the precipitation systems of the four size categories. Next, the rainfall amounts for each class were accumulated separately. In the figure, the different colors denote the contributions from the different rainfall classes: moderate rain (gray), severe precipitation systems of $S < 10^2$ km^2 (blue), $S = 10^2$–10^3 km^2 (cyan), $S = 10^3$–10^4 km^2 (magenta), and $S \geq 10^4$ km^2 (yellow). From Fig. 3a, we note that in the Hiroshima domain, the rainfall corresponding to the largest precipitation system ($S \geq 10^4$ km^2) contributes to about one-third of the total rainfall amount. In particular, about 60 % of the 72-h total rainfall appears to have occurred just in 18 h between 0600 UTC 6 July and 0000 UTC 7 July, about 60 % of which was caused by the largest precipitation systems. Figure 4 shows area-averaged rainfall amount for every six hours from 1200 UTC 4 July to 1200 UTC 7 July 2018. Large precipitation systems of $S \geq 10^4$ km^2 caused remarkably large amounts of rainfall for the 6-h periods from 0600 UTC 6 July and from 1800 UTC 6 July in the Hiroshima domain (yellow bars in

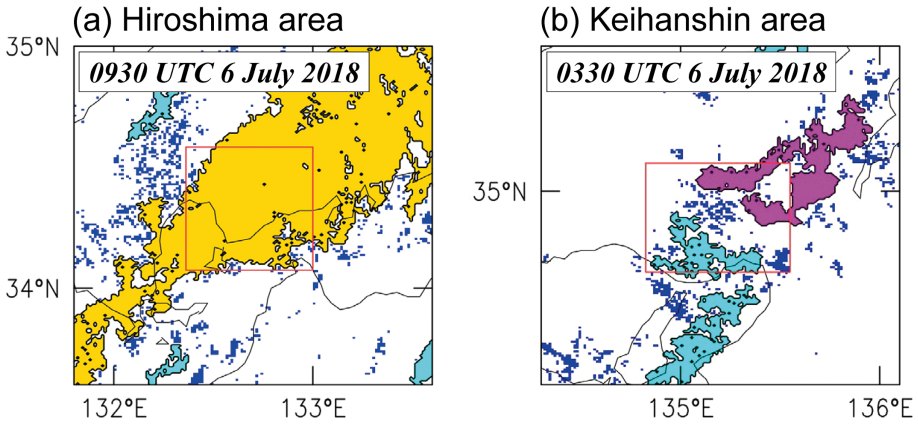

Fig. 5. Examples of precipitation systems passing through (a) the Hiroshima area and (b) the Keihanshin area. (a) Snapshot at 0930 UTC 6 July 2018 and (b) snapshot at 0330 UTC 6 July 2018. Blue, cyan, magenta, and yellow colors indicate precipitation systems with $S < 10^2$ km^2, $S = 10^2$–10^3 km^2, $S = 10^3$–10^4 km^2, and $S \geq 10^4$ km^2, respectively, where S denotes the area of the precipitation system. Red frames in each panel indicate the present study's analysis domains.

Fig. 4a). Such a rapid accumulation of rainfall may have caused many sediment disasters in the Hiroshima area. On the other hand, from Fig. 3b, we observe that in the Keihanshin domain, almost half of the total rainfall appears to have been caused by moderate precipitation ($P < 10$ mm h^{-1}). Furthermore, when we focus on severe rain ($P \geq 10$ mm h^{-1}), the contribution from smaller precipitation systems is relatively large compared with that in the Hiroshima domain. Consequently, the rapid accumulation of rainfall as in the Hiroshima area did not occur in the Keihanshin area.

Figure 5 shows a typical case of the detected precipitation systems in the Hiroshima and Keihanshin areas. As Fig. 5a, we note that significantly large precipitation systems of $S \geq 10^4$ km^2 often covered the Hiroshima area, particularly during the 18 hours from 0600 UTC 6 July to 0000 UTC 7 July. On the other hand, in the Keihanshin area, smaller precipitation systems were dominant (Fig. 5b). Some large precipitation systems of $S \geq 10^4$ km^2 also passed through this area, but their impact was significantly smaller (Figs. 3, 4). We speculate that the difference in damage between the Hiroshima and Keihanshin areas was strongly related to the differently-sized typical precipitation systems striking these two areas. We further discuss the potential risk due to large precipitation systems in Section 4.

3.2 *Background atmospheric conditions in Hiroshima and Keihanshin areas*

Figure 6 shows time series of the CAPE, KI, $\Delta V_{0.5-2.5}$, and $\Delta V_{2.5-6.0}$ averaged both in the Hiroshima (red) and Keihanshin (blue) domains. The figure also depicts the time series of the average value for the pre-12-h period (thick translucent lines). We note from the figure that the CAPE in the Hiroshima domain was small throughout the heavy rainfall event (red line in Fig. 6a). On 6 July, when the destructive rainfall due to large precipitation systems occurred in the Hiroshima domain, CAPE in this domain was only 53 J kg^{-1} on average. This result indicates that the background atmospheric profile around the Hiroshima area on 6 July was nearly neutral to moist convection, although CAPE increased slightly when large precipitation systems caused the destructive rainfall. In the Keihanshin domain on 6 July, CAPE was moderate, but significantly larger than in the Hiroshima domain (blue line in Fig. 6a). The KI was high throughout the event in both domains (Fig. 6b). The average KI in 72 hours from 1200 UTC 4 July to 1200 UTC 7 July was about 37°C (36°C) in the Hiroshima (Keihanshin) domain: This value is comparable with the most frequent value for the environmental conditions of quasi-stationary convective clusters in Japan (Unuma and Takemi 2016). On 6 July, KI in the Hiroshima domain was higher than in the Keihanshin domain although CAPE was considerably lower, thereby implying a relatively small temperature lapse rate and abundant low-to-mid-level moisture in the Hiroshima domain. In this regard, Hamada et al. (2015) have shown that the heaviest rainfall is related to less conditionally and convectively unstable and wetter environments. The

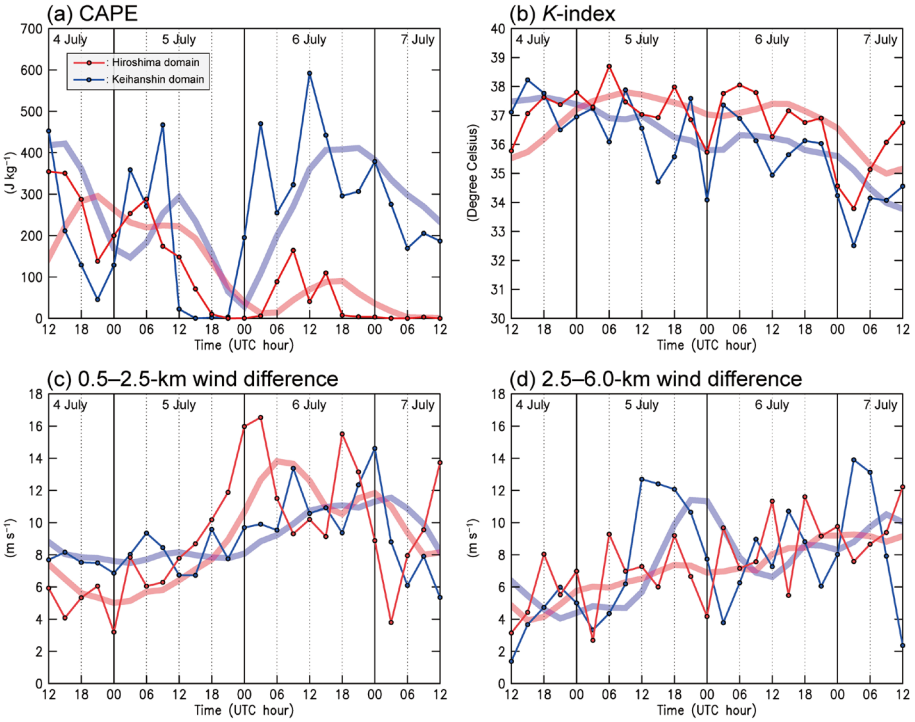

Fig. 6. Time series of (a) convective available potential energy (CAPE), (b) *K*-index, (c) wind difference between 0.5 and 2.5 km above ground level (AGL), and (d) wind difference between 2.5 and 6.0 km AGL from 1200 UTC 4 July to 1200 UTC 7 July 2018 in the analysis domains. Red lines indicate the Hiroshima domain, and the blue lines indicate the Keihanshin domain. The thick, translucent lines indicate the time series of the average value for the pre-12-h period.

background atmospheric condition in the Hiroshima domain on 6 July probably corresponds to a "heaviest rainfall" environment. As for vertical wind shear, the low-level one ($\Delta V_{0.5-2.5}$) increased on 6 July in the Hiroshima domain (red lines in Fig. 6c): $\Delta V_{0.5-2.5}$ reached the largest value of 16.5 m s^{-1} at 0300 UTC 6 July, and the average $\Delta V_{0.5-2.5}$ on July 6 in the Hiroshima domain was 12.2 m s^{-1}, which is larger than the average values on the other days (July 4, 5, and 7). The mid-level shear ($\Delta V_{2.5-6.0}$) had an increasing trend from 1200 UTC 4 July to 1200 UTC 7 July in the Hiroshima domain (red lines in Fig. 6d). Although $\Delta V_{2.5-6.0}$ reached the maximum at 1200 UTC 7 July, the average $\Delta V_{2.5-6.0}$ of each day in the Hiroshima domain becomes largest on 6 July because $\Delta V_{2.5-6.0}$ decreased sharply after 1200 UTC 7 July (not shown). In the Hiroshima domain, the destructive rainfall caused by large precipitation systems occurred under a high vertical wind shear environment. In the Keihanshin domain, while the peak value of $\Delta V_{0.5-2.5}$ was smaller than that of the Hiroshima domain (blue line in Fig. 6c), the $\Delta V_{2.5-6.0}$ value was comparable, or even sometimes significantly larger (blue line in Fig. 6d). This result indicates that a high vertical wind shear environment does not always result in the formation of large precipitation systems. We also note that the area of the analysis domain (3309 km^2) is significantly less than that of large precipitation systems ($O(10^4$ km^2)); thus, the atmospheric profile in the analysis domain does not necessarily correspond to the environment of each precipitation system. The following section focuses on further statistical analysis to elucidate the preferable conditions for large precipitation systems.

4. Discussion

4.1 Potential risk due to large precipitation systems

The rainfall caused by large precipitation systems ($S \geq 10^4$ km^2) seems to be strongly related to the catastrophic damage observed in the Hiroshima area. Here, we discuss the potential risk due to large precipitation systems. Figure 7 shows the distribution of the mean rainfall intensity of each precipitation system

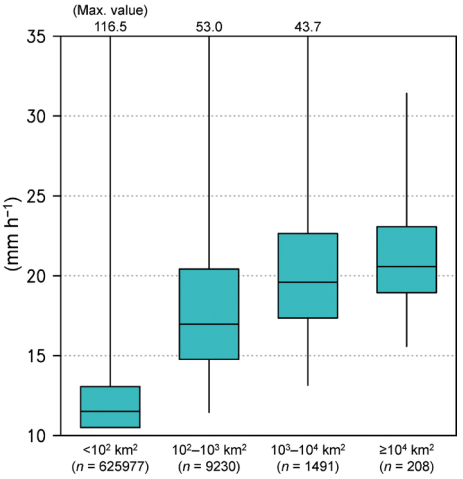

Fig. 7. Box-and-whisker plots for mean rainfall intensity of each precipitation system detected in western Japan from 1200 UTC 4 July to 1200 UTC 7 July 2018. Each plot from left to right shows the distribution for precipitation systems with $S < 10^2$ km^2, $S = 10^2$–10^3 km^2, $S = 10^3$–10^4 km^2, and $S \geq 10^4$ km^2, respectively, where S denotes the area of the precipitation system.

detected in western Japan from 1200 UTC 4 July to 1200 UTC 7 July 2018 in the form of box-and-whisker plots for each size category. The precipitation system's mean rainfall intensity tends to become stronger as its size increases. In general, the rainfall amount at a certain location is determined by both the average rainfall intensity and duration (Doswell et al. 1996). For the heavy rainfall in July 2018, larger precipitation systems tended to exhibit stronger rainfall intensities, thus having the potential to cause a greater rainfall amount for the same duration. The rainfall duration caused by each precipitation system is unknown. However, we suppose that it takes more time for larger precipitation systems to pass a certain location. In our classification, the precipitation system area is categorized by the tenfold increase, corresponding to 3.2 times difference in horizontal length scale. If the systems' propagation speeds are not significantly different among the different size categories, the rainfall durations caused by larger precipitation systems are longer.

From Fig. 7, the difference in the rainfall intensity between the categories of $S = 10^3$–10^4 km^2 and $S \geq 10^4$ km^2 is significantly smaller than this difference between other categories. This implies that precipitation systems with areas larger than $O(10^3$ km$^2)$ consist of multiple smaller ($S < O(10^3$ km$^2)$) precipitation systems having similar rainfall intensities. Kato (2006) revealed that precipitation system observed over northern Kyushu on 29 June 1999 had a hierarchical structure from individual convective cells to mesoscale convective systems (MCSs). It is plausible that large precipitation systems of $S \geq 10^4$ km^2 detected in our study correspond to such MCSs and have a similar hierarchical structure to that elucidated by Kato (2006). In the case of the Kyushu heavy rainfall in 1999, the MCSs' propagation speeds were much slower than those of individual convective cells (Kato 2006). Thus, large precipitation systems here can also have slower propagation speeds, and rainfall durations caused by large precipitation systems become even longer.

A continuous, intense rainfall causes its rapid accumulation. It will lead to a rapid increase in the soil water content considering the simple tank model (e.g., Ishihara and Kobatake 1979), which may result in sediment disasters. In the Hiroshima area, intense, and possibly continuous, rainfall caused by large precipitation systems led to a very rapid increase in the accumulated rainfall, thereby enhancing the risk of sediment disasters in this area. On the other hand, in the Keihanshin area, the passage of smaller precipitation systems (Fig. 5b) resulted in more intermittent rainfall, which led to less enhancement of soil water content relative to the Hiroshima area. We suggest that the destructive damage in the Hiroshima area was mainly caused by large precipitation systems of $S \geq 10^4$ km^2.

4.2 Impact of large precipitation systems in western Japan

To discuss the risk due to large precipitation systems of $S \geq 10^4$ km^2 more generally, we evaluate large precipitation systems' impact on rainfall amounts in western Japan during the heavy rainfall event. Figure 8 shows the accumulated rainfall amount due to large precipitation systems during the 72 hours from 1200 UTC 4 July to 1200 UTC 7 July and its ratio relative to the total rainfall amount in the same period. The rainfall amount caused by large precipitation systems was significantly large in northern Kyushu Island, western Shikoku Island, and the rainfall area extended from the Hiroshima area to its northeast (Fig. 8a). Its contribution to the total rainfall was also large in these areas (Fig. 8b). Among these, the area including the Hiroshima domain was the most widely affected by large precipitation systems. We note here that there were 413 sediment disasters in Ehime Prefecture,

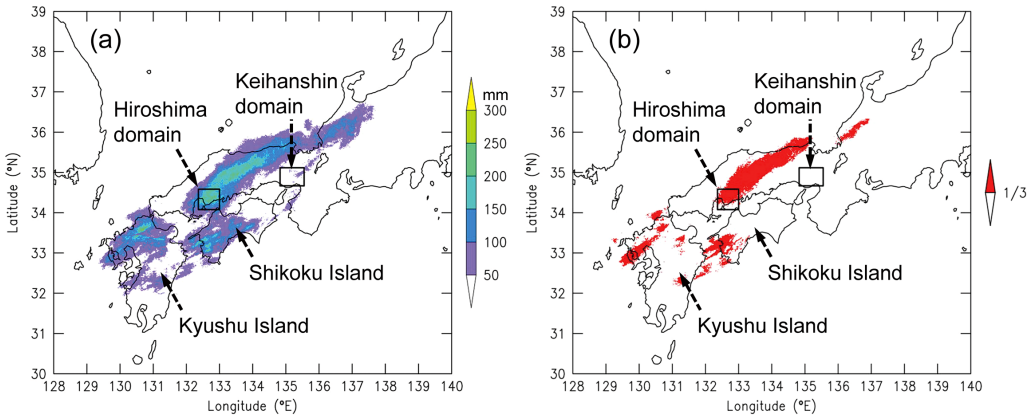

Fig. 8. Impact of large precipitation systems ($S \geq 10^4$ km^2) on rainfall amounts in western Japan during the heavy rainfall event. (a) Accumulated rainfall amount caused by large precipitation systems from 1200 UTC 4 July to 1200 UTC 7 July 2018. (b) Regions with rainfall amount greater than one-third of the total rainfall amount shown in Fig. 1b.

located in western Shikoku Island, which was next only to the number of sediment disasters in Hiroshima Prefecture (Cabinet Office 2019). In three prefectures in northern Kyushu Island (Nagasaki, Saga, and Fukuoka prefectures), there were 198 sediment disasters, which was almost twice that in the Keihanshin area (Cabinet Office 2019). In these areas, rapid accumulation of rainfall, caused by large precipitation systems, possibly led to deadly disasters. We speculate that the sediment disasters during the heavy rainfall event were strongly related to continuous intense rainfall caused by large precipitation systems. However, a more detailed analysis of the link between precipitation system characteristics and local damage in western Japan during the heavy rainfall event is necessary. This will be addressed in future studies.

4.3 *Preferable conditions for large precipitation systems*

To examine the preferable conditions for the formation of large precipitation systems, we performed a simple statistical analysis. Figure 9 shows the box-and-whisker plots for the CAPE, KI, $\Delta V_{0.5-2.5}$, and $\Delta V_{2.5-6.0}$ for the precipitation systems of each size category detected in western Japan (the red-framed region in Fig. 1a) from 1200 UTC 4 July to 1200 UTC 7 July 2018. The values of these indices for each precipitation system are defined as their averages within the area enclosed by the edge of each system. The three plots in each panel indicate the distributions for the precipitation systems of $S = 10^2$–10^3 km^2 (left), $S = 10^3$–10^4 km^2 (middle), and $S \geq 10^4$ km^2 (right). The sample size of each category was 9230, 1491, and 208 in that order. As can be inferred from Fig. 6, the background atmospheric fields of the precipitation systems appearing in the heavy rainfall event are characterized by small CAPE and high KI values (Figs. 9a, b, respectively). However, there is no systematic trend in both the CAPE and KI values with respect to the size of the precipitation system. This result indicates that the size of the precipitation system does not depend on CAPE and KI, at least for the heavy rainfall event in July 2018, although a high KI environment affords preferable conditions for moist convection. On the other hand, there is a clear trend in vertical wind shear (Figs. 9c, d). The 25th percentile values (bottom of the green box) for the largest-size group are larger than the median values (horizontal bar in the green box) for the other groups. Hence, for the heavy rainfall event in July 2018, we can state that a high vertical wind shear environment provided preferable conditions for the formation of large precipitation systems with areas equal to or larger than 10^4 km^2. In general, vertical wind shear is necessary to generate and maintain organized convective systems, such as multicell storms or squall lines. For example, in a conditional unstable environment, low-level vertical wind shear works on generating new convective cells successively by inducing the convergence of old-cell-generated cold pools and warm moist air in front of the old cells, thus resulting in convective organization (Weisman and Klemp 1982; Rotunno et al. 1988). Such a mechanism is probably related to the formation of large precipitation systems having

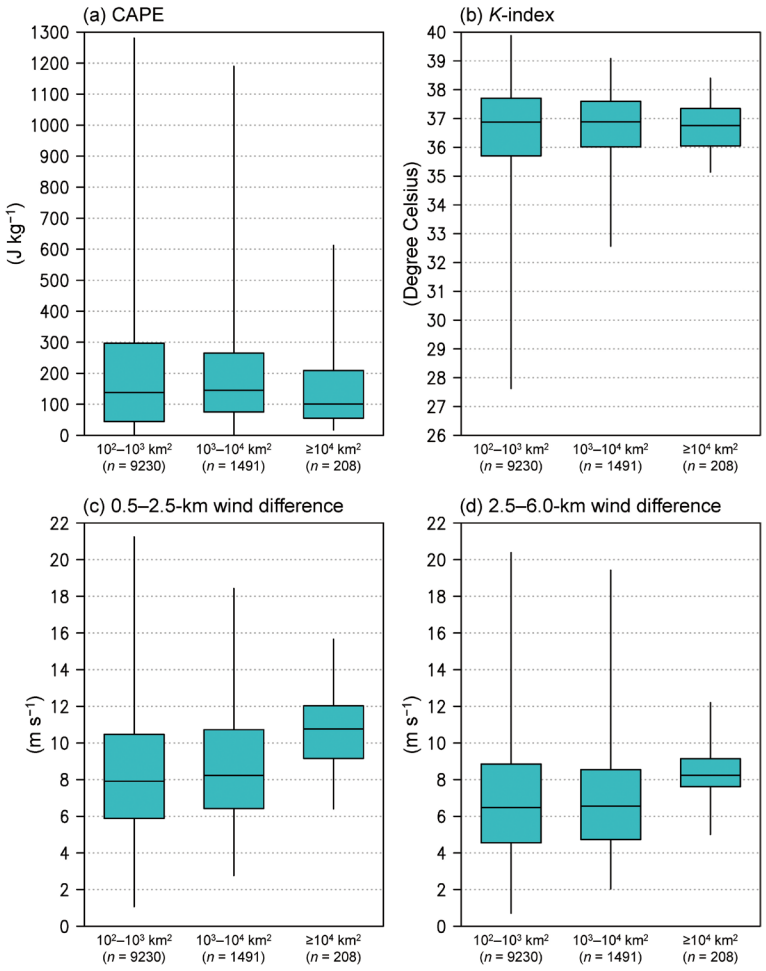

Fig. 9. Box-and-whisker plots for (a) convective available potential energy (CAPE), (b) *K*-index, (c) wind difference between 0.5 and 2.5 km above ground level (AGL), and (d) wind difference between 2.5 and 6.0 km AGL for each precipitation system detected in western Japan from 1200 UTC 4 July to 1200 UTC 7 July 2018. The values for each precipitation system are defined as their averages within the area enclosed by the edge of each system. In each panel, the left, middle, and right plots show the distributions for precipitation systems with $S = 10^2$–10^3 km^2, $S = 10^3$–10^4 km^2, and $S \geq 10^4$ km^2, respectively, where S denotes the area of the precipitation system.

the hierarchical structure like MCSs observed in the Kyushu heavy rainfall in 1999 (Kato 2006). Furthermore, vertical vorticity, generated by tilting the horizontal vorticity associated with low-to-mid-level vertical wind shear, can enhance the longevity and intensity of each convective cell in precipitation systems, thus leading to strong rainfall intensity in large precipitation systems (Fig. 7). The hodograph shape for environmental wind were not investigated in this study; however, this, in addition to the magnitude of shear, also impacts the convective storm characteristics. This will be addressed in future studies.

5. Conclusions and remarks

We examined rainfall intensity data during the extreme heavy rainfall event in western Japan in July 2018 in order to clarify the reason underlying the damage difference between the Hiroshima and Keihanshin areas, despite the fact that both these areas experienced almost the same amount of total rainfall. In the Hiroshima area, large precipitation systems, with an area equal to or larger than 10^4 km^2, caused a rapid increase in accumulated rainfall amounts. This significantly enhanced the risk of deadly sediment disasters in the Hiroshima area. In contrast, in the

Keihanshin area, almost half of the total rainfall was caused by moderate rain where the rainfall intensity was less than 10 mm h^{-1}, and another portion of rainfall was due to intermittent severe rain caused by relatively small precipitation systems. Hence, the increased rate of the accumulated rainfall during the event in the Keihanshin area was considerably smaller, which resulted in less damage. We also examined the background atmospheric conditions in the Hiroshima and Keihanshin areas, applying the indices of CAPE, KI, and low- and mid-level vertical wind shear, to study the factors contributing to the formation of large precipitation systems. The destructive rainfall period in the Hiroshima area was characterized by high KI and a high vertical wind shear environment. We also focused on the statistics relevant to these indices for precipitation systems appearing throughout the heavy rainfall event. The results show that the precipitation system's size mostly depends on the vertical wind shear's magnitude.

Our findings imply that the degree of local damage through widely ranging, long-lasting heavy rainfall largely depends on the size of the precipitation systems striking each area. In particular, the formation of large precipitation systems appears to significantly increase the disaster risk, which can be assessed by examining the magnitude of the vertical wind shear. However, we note here that other factors probably affect the differences in precipitation systems in addition to the mesoscale background conditions. For example, the coupling of an atmospheric river and an upper-level disturbance can affect the formation of heavy precipitation systems (Hirota et al. 2016). Local topography can also enhance lifting of low-level air and consequent heavy rainfall (Watanabe and Ogura 1987; Yoshizaki et al. 2000). Furthermore, low-level moisture supply to a stationary front is necessary for the successive generation of convective clouds (Yoshida et al. 2019). Investigating the influences of these factors on the formation of large precipitation systems can be done in future studies. High-resolution numerical experiments, reasonably simulating the generation of each convective cloud, are desirable to understand the formation mechanism of large precipitation systems. It is necessary to further investigate the essence of large precipitation systems that cause catastrophic damage to human society.

Supplements

Supplement 1 compares the rainfall amounts estimated by the radar data and by the radar/rain-gauge-analyzed precipitation data. Figure S1 shows the time series of the total rainfall rate and the accumulated rainfall amounts estimated by the radar/rain-gauge-analyzed precipitation data. These are to be compared with Figs. 1a and 1b. Figure S2 compares the two datasets for the area-averaged accumulated rainfall in the analysis domains.

Acknowledgments

We thank Dr. Naoko Seino and two anonymous reviewers for many helpful suggestions to improve the manuscript. All datasets were provided by the Japan Meteorological Business Support Center. The radar data and the MA data were collected from the webpage of the Research Institute for Sustainable Humanosphere, Kyoto University (http://database.rish.kyoto-u.ac.jp/arch/jmadata/). We would like to thank Editage (www.editage.jp) for English language editing. This study was supported by the Foundation for Computational Science (FOCUS) Establishing Supercomputing Center of Excellence, JST CREST Grant Number JPMJCR1312, and JST AIP Grant Number JPMJCR19U2, Japan.

References

Cabinet Office, 2019: *Damage by the heavy rainfall in July 2018* (in Japanese). [Available at http://www.bousai.go.jp/updates/h30typhoon7/pdf/310109_1700_h30typhoon7_01.pdf.]

Doswell III, C. A., H. E. Brooks, and R. A. Maddox, 1996: Flash flood forecasting: An ingredients-based methodology. *Wea. Forecasting*, **11**, 560–581.

Hamada, A., Y. N. Takayabu, C. Liu, and E. J. Zipser, 2015: Weak linkage between the heaviest rainfall and tallest storms. *Nat. Commun.*, **6**, 6213, doi:10.1038/ncomms7213.

Hirota, N., Y. N. Takayabu, M. Kato, and S. Arakane, 2016: Roles of an atmospheric river and a cutoff low in the extreme precipitation event in Hiroshima on 19 August 2014. *Mon. Wea. Rev.*, **144**, 1145–1160.

Ishihara, Y., and S. Kobatake, 1979: Runoff model for flood forecasting. *Bull. Disaster Prev. Res. Inst. Kyoto Univ.*, **29**, 27–43. [Available at https://repository.kulib.kyoto-u.ac.jp/dspace/bitstream/2433/124881/1/b29p1n260p02.pdf.]

Japan Meteorological Agency, 2013: *Outline of the operational numerical weather prediction at the Japan Meteorological Agency*. Appendix to WMO Techical Progress Report on the Global Data-Processing and Forecasting System and Numerical Weather Prediction. [Available at http://www.jma.go.jp/jma/jma-eng/jma-center/nwp/outline2013-nwp/index.htm.]

Kato, T., 2006: Structure of the band-shaped precipitation system inducing the heavy rainfall observed over northern Kyushu, Japan on 29 June 1999. *J. Meteor.*

Soc. Japan, **84**, 129–153.

Kato, T., 2018: Representative height of the low-level water vapor field for examining the initiation of moist convection leading to heavy rainfall in East Asia. *J. Meteor. Soc. Japan*, **96**, 69–83.

Nagata, K., 2011: *Quantitative precipitation estimation and quantitative precipitation forecasting by the Japan Meteorological Agency*. RSMC Tokyo–Typhoon Center, Technical Review, **13**, 37–50. [Available at https://www.jma.go.jp/jma/jma-eng/jma-center/rsmc-hp-pub-eg/techrev/text13-2.pdf.]

Rasmussen, E. N., and D. O. Blanchard, 1998: A baseline climatology of sounding-derived supercell and tornado forecast parameters. *Wea. Forecasting*, **13**, 1148–1164.

Rotunno, R., 1981: On the evolution of thunderstorm rotation. *Mon. Wea. Rev.*, **109**, 577–586.

Rotunno, R., J. B. Klemp, and M. L. Weisman, 1988: A theory for strong, long-lived squall lines. *J. Atmos. Sci.*, **45**, 463–485.

Takemi, T., 2006: Impacts of moisture profile on the evolution and organization of midlatitude squall lines under various shear conditions. *Atmos. Res.*, **82**, 37–54.

Thompson, R. L., R. Edwards, J. A. Hart, K. L. Elmore, and P. Markowski, 2003: Close proximity soundings within supercell environments obtained from the rapid update cycle. *Wea. Forecasting*, **18**, 1243–1261.

Tsuguti, H., and T. Kato, 2014: Objective extraction of heavy rainfall events and statistical analysis on their characteristic features. *Tenki*, **61**, 455–469 (in Japanese).

Unuma, T., and T. Takemi, 2016: Characteristics and environment conditions of quasi-stationary convective clusters during the warm season in Japan. *Quart. J. Roy. Meteor. Soc.*, **142**, 1232–1249.

Watanabe, H., and Y. Ogura, 1987: Effects of orographically forced upstream lifting on mesoscale heavy precipitation: A case study. *J. Atmos. Sci.*, **44**, 661–675.

Weisman, M. L., and J. B. Klemp, 1982: The dependence of numerically simulated convective storms on vertical wind shear and buoyancy. *Mon. Wea. Rev.*, **110**, 504–520.

Weisman, M. L., J. B. Klemp, and R. Rotunno, 1988: Structure and evolution of numerically simulated squall lines. *J. Atmos. Sci.*, **45**, 1990–2013.

Wilhelmson, R. B., and J. B. Klemp, 1978: A numerical study of storm splitting that leads to long-lived storms. *J. Atmos. Sci.*, **35**, 1974–1986.

Yoshida, R., S. Nishizawa, H. Yashiro, S. A. Adachi, T. Yamaura, H. Tomita, and Y. Kajikawa, 2019: Maintenance condition of back-building squall-line in a numerical simulation of a heavy rainfall event in July 2010 in western Japan. *Atmos. Sci. Lett.*, **20**, e880, doi:10.1002/asl.880.

Yoshizaki, M., T. Kato, Y. Tanaka, H. Takayama, Y. Shoji, H. Seko, K. Arao, K. Manabe, and Members of X-BAIU-98 Observation, 2000: Analytical and numerical study of the 26 June 1998 orographic rainband observed in western Kyushu, Japan. *J. Meteor. Soc. Japan*, **78**, 835–856.